Supplementary Material for "Infrared Dielectric Function of $GaAs_{1-x}P_x$ Semiconductor Alloys Near the Reststrahlen Bands"

(Dated: 26 August 2023)

Stefan Zollner,¹ Shivashankar R. Vangala,² Vladimir L. Tassev,² Duane Brinegar,^{2,3} and Samuel Linser^{2,3}

S1. DETAILS OF EXPERIMENTAL AND DATA ANALYSIS METHODS

The ellipsometric angles ψ and Δ and the depolarization spectra of several thick $GaAs_{1-x}P_x$ alloy layers deposited on GaAs were acquired at room temperature from 250 to 8000 $\rm cm^{-1}$ using a J. A. Woollam Fouriertransform IR variable angle of incidence spectroscopic ellipsometer (FTIR-VASE). Sample parameters are shown in Table SI. We selected 70° and 75° as the angles of incidence for our measurements, both below and above the mid-IR Brewster angles of the samples. We chose a resolution of 4 cm^{-1} . A smaller resolution increases the data acquisition time and the noise, while a larger resolution broadens the features of the spectra. Our choice of 4 cm⁻¹ seemed a good compromise for these samples. A smaller resolution is required for bulk GaP crystals, especially at low temperatures, ⁶ but alloy disorder and small variations in composition increase our broadenings to values above 4 cm⁻¹. Measurements were performed with 15 compensator positions per revolution. To increase the signal-to-noise ratio, we averaged 200 interferometer mirror scans at each compensator position. Systematic errors were reduced with two $P=\pm 45^{\circ}$ polarizer positions and also zone-averaging the analyzer $(A=0^{\circ}, 90^{\circ})$. A typical measurement took about 18 hours per sample. WVASE32 and CompleteEase (J. A. Woollam Co., Lincoln, NE) ellipsometry software was used to analyze our data.

For each sample, we first restricted the analysis range to 500 to 8000 cm⁻¹. In this range, the ellipsometric angle Δ is close to 0° or 180° and the imaginary part of the pseudodielectric function $\langle \epsilon_2 \rangle$ is very small (below 0.5), see Fig. S2. These data were used to fit the thickness of the surface layer, which we described using the Bruggeman effective medium approximation (BEMA) as a mixture consisting of 50% alloy layer and 50% voids. Typical surface layer thicknesses were between 20 and 50 Å, see Table SI. Next, we fitted the real part of the pseudodielectric function $\langle \epsilon_1 \rangle$ to determine the alloy layer thickness (5 to 30 μ m), the high-frequency dielectric constant ϵ_{∞} , and the thickness nonuniformity (5 to 20%).

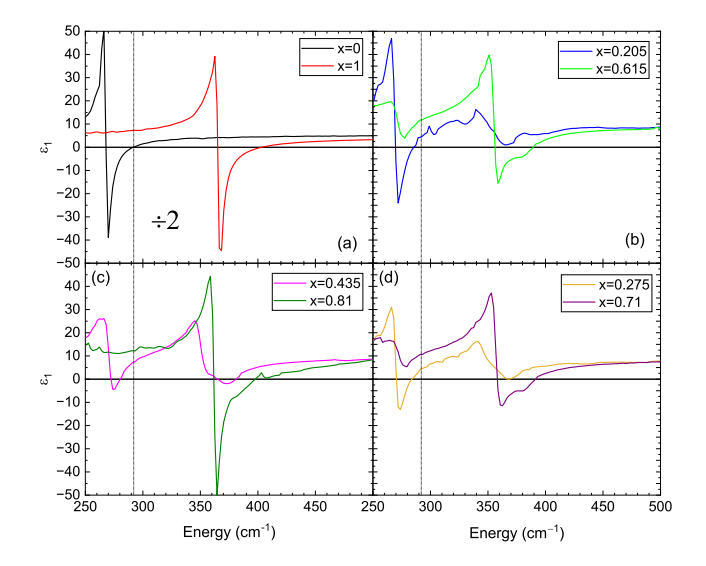


FIG. S1. Real part of the dielectric function ϵ_1 for bulk GaAs and GaP (a) and for thick $\operatorname{GaAs}_{1-x}\operatorname{P}_x$ alloys on GaAs (b,c,d) determined from a B-spline fit to the ellipsometric angles. The spectra were divided by two for the bulk substrates in (a) to fit on the same scale as the alloys. The vertical lines show the LO mode of the GaAs substrate. The corresponding imaginary parts are shown in Fig. 3 in the main text.

These values were then fixed during the subsequent analysis of the phonon reststrahlen bands between 250 and 500 cm⁻¹, but iterative adjustments were sometimes required to achieve acceptable agreement between data and model over the complete spectral range. Since the layers were rather thick and nonuniform, the error was about 0.1 for ϵ_{∞} and about 5-10% for the layer thickness. Perfect agreement between model and data above 500 cm⁻¹ could not be found due to thickness nonuniformity, which is difficult to model. The digital filter (convolution profile) used to describe thickness nonuniformity sometimes caused ringing as a function of photon energy. This was not important for the analysis of the phonon spectra at lower energies.

S2. DETAILED RESULTS FOR SAMPLE 225B WITH 61.5% PHOSPHORUS

The ellipsometry data for a typical sample (225B) with a phosphorus content of 61.5%, within the percolation regime, ¹⁵ are shown in Fig. 1 in the reststrahlen region from 250 to 500 cm⁻¹ in several representations, as ellipsometric angles ψ and Δ , pseudodielectric function $\langle \epsilon \rangle$, and pseudoloss function $-1/\langle \epsilon \rangle$. The depolarization for this sample showed two strong peaks at 286 and 395

¹Department of Physics, New Mexico State University, MSC 3D, P.O. Box 30001, Las Cruces, NM 88003, USA

² Air Force Research Laboratory (AFRL), Sensors Directorate, Wright-Patterson AFB, OH 45433, USA

³KBR, Inc., Beavercreek, OH, 45431, USA

TABLE SI. Parameters of $GaAs_{1-x}P_x$ alloys and fit results, including P content x, As content 1-x, layer thickness t, surface layer thickness t, and high-frequency dielectric constant ϵ_{∞} . The amplitudes A, energies Ω_{TO} , and broadenings Γ_{TO} of the GaAs-like and GaP-like transverse optical (TO) phonons are also given. 90% confidence limits are indicated in parentheses. The last two columns list the direct band gap E_0 and the refractive index n at 2 μ m (0.62 eV) determined from a fit to the ellipsometry data with a parametric semiconductor model.

							GaAs	s-like		GaP-like					
Sample	x	1-x	t	r	ϵ_{∞}	A	Ω_{TO}	$\Gamma_{\rm TO}$	Ω_{LO}	A	Ω_{TO}	Γ_{TO}	Ω_{LO}	E_0	n
			(μm)	(Å)			$({\rm cm}^{-1})$	(cm^{-1})	(cm^{-1})		$({\rm cm}^{-1})$	$({\rm cm}^{-1})$	(cm^{-1})	(eV)	
$GaAs^a$	0	1	NA	93	10.7	1.96(2)	268.2(2)	2.2(2)	291.7	NA	NA	NA	NA	1.42	3.35
205B	0.205	0.795	10.8	36	9.5	1.32(6)	269.9(6)	5.1(8)	288.0	0.80(3)	352.5(7)	23(1)	367.0	1.72	3.24
235B	0.232	0.768	24.3	44	10.2	1.36(3)	270.1(3)	4.6(4)	287.5	0.66(1)	354.9(3)	15(1)	366.2	1.76	3.26
237B	0.24	0.76	22.9	32	10.1	1.30(3)	270.0(3)	4.8(4)	286.9	0.61(1)	355.9(3)	13.2(5)	366.5	1.76	3.26
213B	0.245	0.755	28.8	46	9.8	0.83(2)	271.4(4)	4.6(7)	282.7	1.28(2)	356.2(4)	17.6(6)	378.7	1.76	3.24
$213F^b$	0.275	0.725	33.5	80	9.9	1.83(7)	267.3(6)	6.9(1)	291.0	0.91(2)	352.8(4)	19(1)	368.7	no	isy
208B	0.435	0.565	12.4	45	9.8	0.82(3)	272.6(5)	4.6(6)	283.8	1.07(2)	356.9(3)	14.6(6)	375.9	1.98	3.19
208F	0.475	0.525	11.7	58	9.7	0.73(3)	272.8(5)	3.9(7)	282.9	1.24(2)	358.5(4)	13.7(6)	380.7	2.03	3.18
225B	0.615	0.385	7.3	48	9.5	0.44(3)	272.1(8)	5(1)	278.3	1.55(2)	357.7(4)	13(1)	385.8	2.26	3.13
226B	0.71	0.29	8.9	41	9.5	0.43(3)	273.2(7)	5(1)	279.3	1.61(2)	360.0(3)	10(1)	389.3	2.29	3.13
$209B^b$	0.81	0.19	14	52	8.6	0.19(4)	267(2)	5(f)	269.9	1.83(2)	361.4(4)	9.0(6)	398.0	2.50	3.00
GaP^a	1	0	NA	45	8.9	NA	NA	NA	NA	1.98(1)	364.8(1)	2.0(1)	403.3	2.70	3.03

^aResults from this work are in good agreement with Refs. 3–6. ^bNo specular reflection from a red laser beam.

cm⁻¹, but was small in other areas. The imaginary part of the pseudodielectric function $\langle \epsilon_2 \rangle$ has a deep minimum at 291 cm⁻¹ with negative values. This cannot happen for a bulk sample and we attribute this minimum to the Berreman artifact,^{31,32} which occurs at the LO frequency of the GaAs substrate, shown by the vertical dotted line in Fig. 1. The real part $\langle \epsilon_1 \rangle$ has a strong discontinuity at this energy.

Apart from this Berreman artifact, the pseudodielectric function can mostly be interpreted similar to the dielectric function of a bulk ${\rm GaAs}_{1-x}{\rm P}_x$ alloy. $\langle \epsilon_2 \rangle$ has maxima at 272 and 354 cm⁻¹, which are taken as the TO energies of the GaAs-like and GaP-like phonons, respectively. (Of course, some smaller features are due to the finite layer thickness.) The real part $\langle \epsilon_1 \rangle$ has Kramers-Kronig consistent features expected of two Lorentz oscillators.

The spectrum for sample 225B was fitted with a sum of two Lorentzian oscillators to describe the GaAs-like and GaP-like phonons, shown by dotted lines in Fig. 1. Parameters obtained from the fit are given in Table SI. The corresponding LO energies were estimated from the Lyddane-Sachs-Teller relation (2). Solid (dashed) vertical lines in Fig. 1 show the TO (LO) energies obtained from this fit. There is qualitative agreement, especially for the pseudodielectric function, but the agreement could be better. As expected, two Lorentzians are not sufficient to describe the complex vibrational spectra of the $GaAs_{1-x}P_x$ alloy.

We now focus our attention on the ellipsometric angle ψ for sample 225B. This angle rises initially towards a peak located between 272 and 276 cm⁻¹ (showing a

small dependence on the angle of incidence). This rising slope is identified with the lower edge of the GaAs-like reststrahlen band. This first peak is followed by a second peak at 288 cm⁻¹ associated with the Berreman artifact of the substrate. After a minimum at $325~\mathrm{cm}^{-1}$ due to interference effects, ψ rises again towards a doublepeak from 350 to 400 cm⁻¹. This is the GaP-like reststrahlen band. The fit to this GaP-like band with a single Lorentzian (dotted) is particularly poor. As discussed by Humlíček, ^{9,30} the impact of a weak absorption feature is amplified, if it occurs within a reststrahlen band. The shape of this GaP-like reststrahlen band allows the conclusion that the main GaP-like TO/LO phonon pair has energies of about 355 and 400 cm^{-1} , with a second weaker absorption peak located within these boundaries. It is difficult to interpret the ellipsometric angle Δ , because it changes very rapidly with photon energy and wraps around by 2π four times within our spectral window. Finally, we discuss the loss function for sample 225B. As shown in Fig. 1, $\operatorname{Im}(-1/\langle \epsilon \rangle)$ has strong peaks near, but not exactly at the LO frequencies.

In summary, the main features of the raw ellipsometry data in Fig. 1 for sample 225B can be interpreted if the GaAs-like and GaP-like reststrahlen bands and the Berreman artifact at the TO energy of the GaAs substrate are taken into account. There are also small modifications due to the finite thickness of the alloy (interference effects).

Since a fit to the data with two Lorentzians to describe the GaAs-like and GaP-like vibrations was only partially successful, we added a second (weaker) GaP-like TO phonon, as suggested by the percolation theory

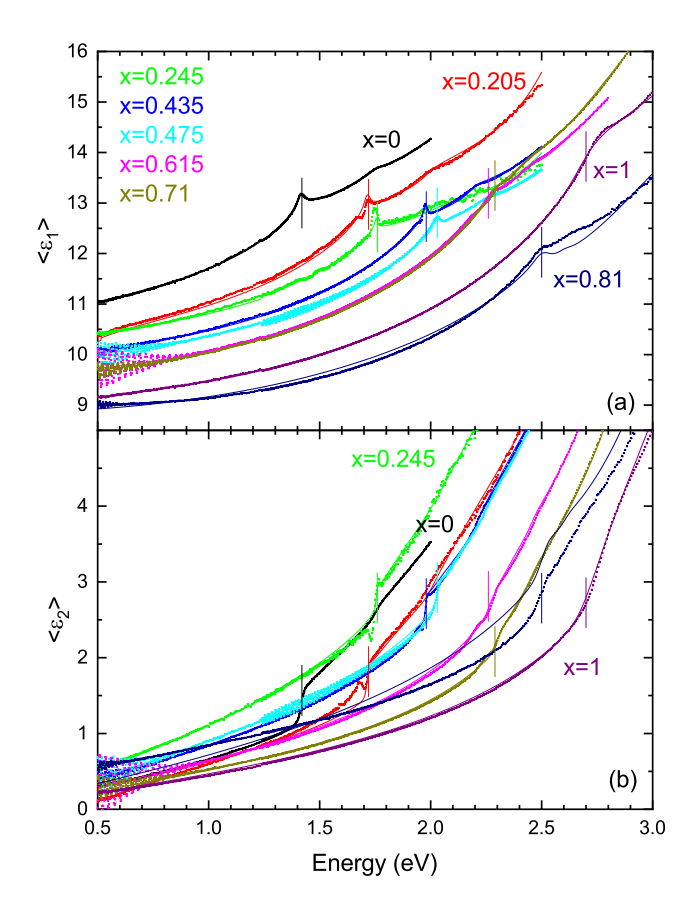


FIG. S2. Real (a) and imaginary part (b) of the pseudodielectric function $\langle \epsilon \rangle$ for selected concentrations of $\mathrm{GaAs}_{1-x}\mathrm{P}_x$ alloy layers on GaAs. Data are shown by symbols. The lines represent the best fit with a parametric semiconductor model as described in the text. The short vertical lines show the location of the direct band gap E_0 obtained from the fit.

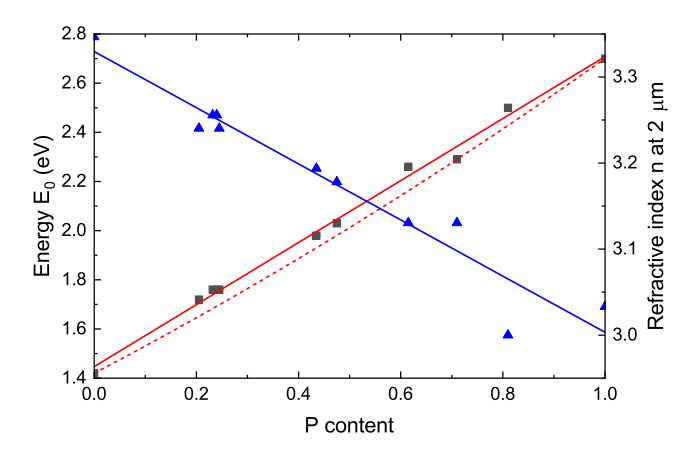


FIG. S3. Direct band gap E_0 (\blacksquare) and refractive index n at a wavelength of 2 μ m (\blacktriangle) of thick $GaAs_{1-x}P_x$ alloys on GaAs as a function of P content, determined from ellipsometry. The solid lines show a linear fit, the dashed line includes a bowing parameter of b=-0.19 eV for the variation of the direct band gap with composition.

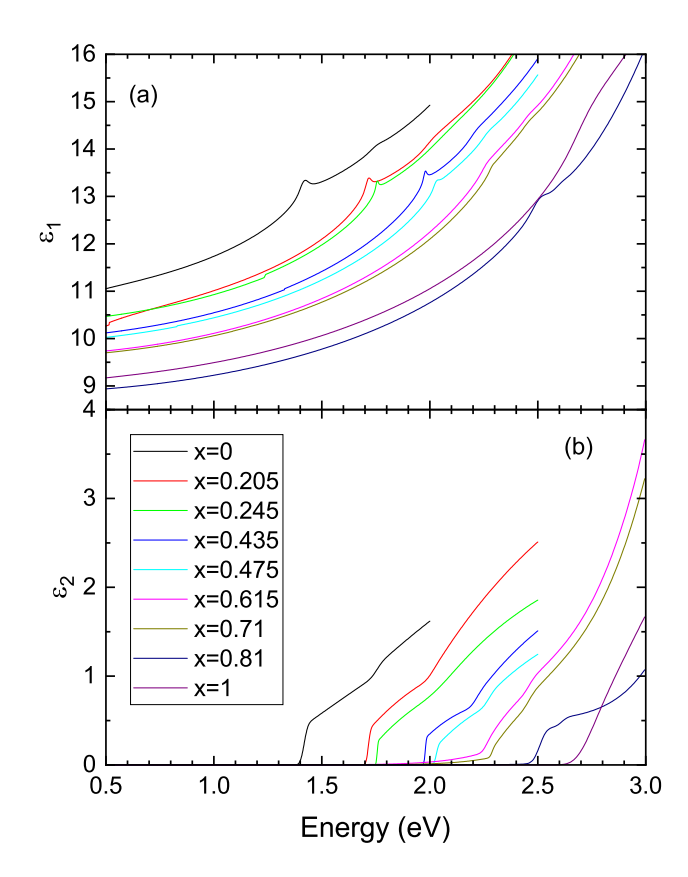


FIG. S4. Real (a) and imaginary part (b) of the dielectric function ϵ for selected concentrations of $GaAs_{1-x}P_x$ alloy layers on GaAs, determined from a parametric semiconductor oscillator fit as described in the text.

of Pagès et al.¹⁵, at an energy of about 12 cm⁻¹ above the stronger one. This reduced the mean standard deviation (weighted by errors), also called MSE, by about 20%, but still did not provide a good description of ψ in the GaP-like reststrahlen region.

The agreement between the model and the data for sample 225B can be improved further if a total of eight Lorentzian oscillators are introduced to describe the lattice absorption. Results are shown by the solid lines in Fig. 1. Even such a large number of oscillators does not achieve a perfect fit to the data. It is questionable whether such a large number of Lorentzian parameters carries physical significance. We believe that our FTIR ellipsometry data do not contain enough information to perform meaningful fits with 6 to 10 Lorentzian for comparison with energies and amplitudes predicted by the cluster model theory, which was carried out in Ref. 14.

S3. ADDITIONAL FIGURE

Figure 3 in the main text showed only the imaginary part of the dielectric function in the reststrahlen region. The corresponding real part is shown in Fig. S1.

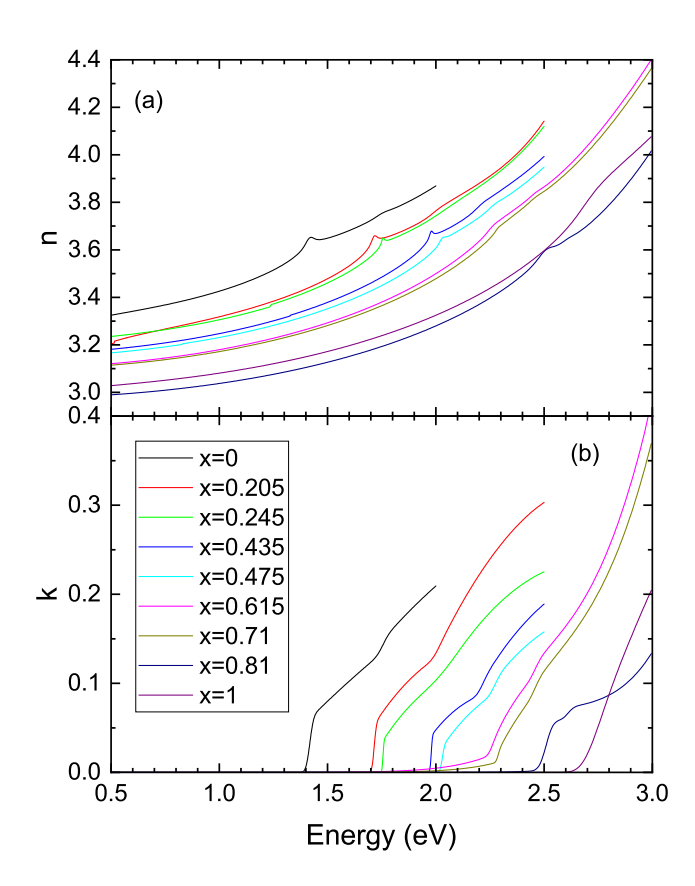


FIG. S5. Same data as in Fig. S4, but displayed as the real (a) and imaginary part (b) of the complex refractive index n+ik for selected concentrations of $GaAs_{1-x}P_x$ alloy layers on GaAs, determined from a parametric semiconductor oscillator fit as described in the text.

S4. ELLIPSOMETRY NEAR THE DIRECT BAND GAP

The ellipsometric Mueller matrices from 55° to 80° in 5° incremenents were also acquired from 210 to 2500 nm on a J.A. Woollam dual rotating compensator ellipsometer (model RC2-XI+) with 60 s integration time per angle. The ellipsometric angles (diagonal blocks of the Mueller matrices) were fitted with two M_0 parametric semiconductor oscillators for the E_0 and $E_0 + \Delta_0$ critical points. For P contents above 60\%, an M_1 oscillator for the E_1 critical point was also added. The $E_0 + \Delta_0$ critical point was barely noticable in the spectra due to broadening. Therefore, Δ_0 was interpolated linearly with composition between the binary end points and treated as a fixed parameter. The fit range was restricted from 0.5 to 2.5 eV for the lower P contents and 0.5 to 3.0 eV for the higher P contents. The surface layer thickness was treated as an additional parameter using the Bruggeman effective medium approximation with a 50% void fraction, with results similar to those given in Table SI. For the thinner samples, weak interference fringes were noticed at the longest wavelengths. Those were ignored in the modeling and the alloy was taken as a bulk substrate.

The resulting pseudodielectric functions near the di-

rect band gap are shown in Fig. S2. In general, the E_0 critical point can clearly be identified as a peak in the $\langle \epsilon_1 \rangle$ spectra for direct alloys (x<45%). It also leads to a step in $\langle \epsilon_2 \rangle$. For the indirect alloys (x>45%), the short intervalley scattering times from the Γ -point to the X-valleys broaden the E_0 critical point significantly.^{26,33} That makes it more difficult to locate the direct band gap E_0 for the indirect alloys. We rely more on the data fitting procedure for these alloys to find E_0 . We have marked the location of the E_0 gaps with short vertical lines in Fig. S2. The monotonic increase of E_0 with P content x is quite apparent. For some alloys, especially x=0.205 and x=0.435, the direct band gap E_0 has some fine structure caused by the compositional variations in the layers. The band gap of bulk GaAs was found to be 1.42 eV, as expected. The band gap of bulk GaP (2.70 eV) was about 0.08 eV lower than expected.^{33,34} Most likely, this is due to doping. The LO phonon energy for this bulk GaP substrate was also found to be larger than expected, see Table SI, consistent with a plasma frequency of 60 cm^{-1} and an electron concentration on the order of 1.3×10^{17} cm⁻¹, see Ref. 35. The broadening of the E_0 critical point for this bulk GaP substrate is also larger than expected.³³ (A detailed lineshape analysis using deriatives is not possible with RC2 ellipsometry data.)

The pseudo-refractive index at long wavelengths (the square root of $\langle \epsilon_1 \rangle$) also increases monotonically with P content, with the exception for the alloy with 81% P. The composition of this alloy seems correct, as given by the location of the direct band gap E_0 . However, its refractive index is lower than it should be. Most likely, this alloy has embedded voids, which reduce the refractive index following the Bruggeman effective medium theory.

The location of the direct band gap can also be identified by steps in the $\langle \epsilon_2 \rangle$ spectra, especially for the direct alloys with $x{<}0.45$. On the other hand, the magnitude of the $\langle \epsilon_2 \rangle$ spectra at low energies depends mostly on the surface roughness and therefore varies greatly between samples with no apparent trends.

The direct band gap E_0 and the refractive index n at 2 μ m wavelength are listed in Table SI and also plotted in Fig. S3 as a function of composition. The rise of E_0 is nearly linear with increasing P content, as shown by the solid line. Our errors are too large to determine the bowing parameter. The expected dependence²⁶ of E_0 versus P content with a bowing parameter of b=-0.19 eV is shown by the dotted line, which is not unreasonable in comparison with our results. The decrease of n at 2 μ m wavelength is also nearly linear, as shown by the solid line. The only exception is the sample with 81% P. It has already been discussed that the low refractive index for this sample is probably due to voids, which result in a relatively lower electron density.

For completeness, we also show the complex dielectric function ϵ and the complex refractive index n+ik obtained from the parametric semiconductxor models in Figs. S4 and S5, respectively. No attempts were made to

clean the surfaces, reduce overlayers, or improve the accuracy of the data. Since the agreement with the model and the fit is not always perfect, the data shown in these figures needs to be taken with a grain of salt. They are qualitatively correct, but small deviations should be expected due to the built-in numerical "features" of the parametric semiconductor model. The data confirm the much lower broadenings for the direct alloys with P contents below 45% than for the indirect alloys. We also see systematic variations of the refractive index and the

direct band gap with increasing P content, except for the 81% sample as mentioned above. The alloys with 61.5% and 71% P seem to show absorption below the band gap, but ellipsometry is not really sensitive to low-level indirect absorption processes. While certainly plausible, this might be a numerical artifact. The $E_0 + \Delta_0$ transition is more pronounced in ϵ_2 than in the raw experimental data expressed as a pseudodielectric function $\langle \epsilon_2 \rangle$, but this might also be a numerical artifact due to the built-in bias of the parametric semiconductor model.